Electronic Supplementary Information (ESI)

A New Iodate-Phosphate Pb$_2$(IO$_3$)(PO$_4$) Achieving Great Improvement in Birefringence Activated by (IO$_3$)$^-$ Groups

Xiao-Han Zhang,[ab] Bing-Ping Yang,*[a] Jin Chen,[a] Chun-Li Hu,[a] Zhi Fang,[a] Zu-Jian Wang [a] and Jiang-Gao Mao*[a]

a. State Key Laboratory of Structural Chemistry, Fujian Institute of Research on the Structure of Matter, Chinese Academy of Sciences, Fuzhou 350002, P. R. China.
b. College of Chemistry and Materials Science, Fujian Normal University, 32 Shangsan Road, Fuzhou 350007,PR China.
Email: ybp@fjirsm.ac.cn; mjg@fjirsm.ac.cn

Table of Contents

S1. Experimental Section

Synthesis

K_2CO_3 (99.99%, Aladdin), PbO (99.99%, Aladdin), I_2O_5 (99.5%, Shanghai Chemical reagents Co. Ltd.), CF_3COOH (99%, Aladdin), and H_3PO_4 (85% solution, Shanghai Chemical reagents Co. Ltd.) were purchased and used without further purification.

Single crystals of $Pb_2(PO_4)(IO_3)$ were obtained hydrothermally from a mixture of PbO (1 mmol), I_2O_5 (0.45 mmol), H_3PO_4 (15μL), K_2CO_3 (0.35 mmol), CF_3COOH (15μL) and H_2O (1 mL) in a 23 mL Teflon-lined autoclave. The autoclaves were heated to 180 ℃ in 6h, held at that temperature for 4 days, and then cooled to 30 ℃ at a rate of 3 ℃/h. Colorless block crystals of $Pb_2(PO_4)(IO_3)$ were collected by filtration, washed thoroughly with deionized water, and then dried in air. The yield was about 65% based on Pb. The high purity of the polycrystalline products was verified by powder X-ray diffraction (PXRD) (Figure S1).

Single-Crystal X-ray Diffraction (XRD)

Single-crystal X-ray diffraction data were collected on an Agilent Technologies SuperNova dual-wavelength CCD diffractometer with Mo Kα radiation (λ =0.71073 Å) at 293 K. Data reduction was performed using CrysAlisPro, and absorption correction was carried out based on the analytical numeric method.[1] Using Olex2,[2] the structure was solved with the ShelXT[3] structure solution program using Intrinsic Phasing and refined with the ShelXL[4] refinement package using full-matrix least-squares fitting on F^2. The PLATON program[5] was used to check the correctness of the structure. Crystallographic data are summarized in Table 1. Selected bond lengths are listed in Table 2.

Physical Measurements

Powder X-ray diffraction (XRD) pattern was recorded on a MiniFlex600 diffractometer with graphite-monochromated Cu Kα radiation in the 2θ range of 10−70° at room temperature. Elemental analyses were performed on a field emission scanning electron microscope (JSM6700F) equipped with an energy dispersive X-ray spectroscope (EDS Oxford INCA). Infrared (IR) spectra were recorded on a Magna 750 FT-IR spectrometer in the form of KBr pellets in the range 3900 to 400 cm^{-1} at room temperature. The UV−vis−NIR diffuse reflectance spectra were collected on a PE-Lambda 900 UV-vis-NIR spectrophotometer in the range 200−2500 nm at room temperature. Thermogravimetric analysis (TGA) measurements were performed on a NETZSCH STA 499C instrument. The samples were loaded in an Al_2O_3 crucibles and heated from 30 to 1000 ℃ at a rate of 15 ℃ min^{-1} under a

nitrogen atmosphere. The birefringence was characterized by using the ZEISS Axio Scope.A1 Polarized Light Microscope equipped with Berek compensator. The wavelength of the light source was 546 nm. The formula for the calculation of birefringence can be expressed as follows: ΔR(retardation) = $\Delta n \times T$, where ΔR represents the optical path difference, Δn denotes the birefringence, and T denotes the thickness of the crystal. The positive and negative rotation of compensatory can determine the retardation.

Table S1. Crystallographic data for $Pb_2(PO_4)(IO_3)$.

formula	$Pb_2(PO_4)(IO_3)$
formula weight	684.25
crystal system	monoclinic
space group	$P2_1/n$
a/Å	7.3740(3)
b/Å	6.8144(3)
c/Å	13.6077(5)
α/deg	90
β/deg	104.973(4)
γ/deg	90
V/Å^3	660.56(5)
Z	4
D_{calc}/g·cm^{-3}	6.880
μ(Mo Kα)/mm^{-1}	55.812
θ_{max}/deg	27.10
completeness/%	98.6
GOF on F^2	1.027
R_1, $wR2$ [$I > 2\sigma(I)$] [a]	0.0491, 0.1146
R_1, $wR2$ (all data)	0.0557, 0.1213

Table S2. Selected bond lengths (Å) for $Pb_2(PO_4)(IO_3)$.

$Pb_2(PO_4)(IO_3)$			
Bond	Length(Å)	Bond	Length(Å)
I(1)-O(6)	1.823(11)	P(1)-O(3)	1.523(12)
I(1)-O(7)	1.831(10)	P(1)-O(2)	1.538(12)
I(1)-O(5)	1.849(11)	P(1)-O(4)	1.544(12)
Pb(1)-O(2)	2.477(11)	P(1)-O(1)	1.567(11)

Pb(1)-O(3)#1	2.545(12)	Pb(2)-O(1)#1	2.458(10)
Pb(1)-O(6)#4	2.663(10)	Pb(2)-O(7)#2	2.512(10)
Pb(1)-O(5)#2	2.715(11)	Pb(2)-O(2)	2.513(11)
Pb(1)-O(7)#5	2.737(11)	Pb(2)-O(1)#3	2.618(11)
Pb(1)-O(1)	2.752(11)	Pb(2)-O(5)	2.731(12)
Pb(1)-O(5)#1	2.834(13)	Pb(2)-O(4)#3	2.802(12)
Pb(1)-O(7)#1	2.917(10)	Pb(2)-O(4)#4	2.808(11)
Pb(1)-O(3)#5	3.056(12)	Pb(2)-O(6)#2	2.944(12)

Symmetry transformations used to generate equivalent atoms: #1 -x,-y+1,-z+1   #2 x-1/2,-y+3/2,z-1/2   #3 x,y+1,z   #4 -x+1,-y+1,-z+1   #5 x-1/2,-y+1/2,z-1/2   #6 x+1/2,-y+3/2,z+1/2   #7 x,y-1,z   #8 x+1/2,-y+1/2,z+1/2

Table S3. State energies (eV) of the highest valence band (H-VB) and the lowest conduction band (L-CB) of the compound $Pb_2(PO_4)(IO_3)$.

Compound	k-point		H-VB	L-CB
$Pb_2(PO_4)(IO_3)$	Z	(0.000, 0.000, 0.500)	−0.19222	3.61986
	G	(0.000, 0.000, 0.000)	−0.15936	3.60735
	Y	(0.000, 0.500, 0.000)	−0.11041	3.56390
	A	(−0.500, 0.500, 0.000)	−0.12722	3.55015
	B	(−0.500, 0.000, 0.000)	−0.01225	3.15173
	D	(−0.500, 0.000, 0.500)	0	3.13353
	E	(−0.500, 0.500, 0.500)	−0.13588	3.51472
	C	(0.000, 0.500, 0.500)	−0.15344	3.62251

Table S4. Space group, anionic group type, and calculated birefringence of selected phosphates.

Compound	Space group	Anionic group type	Δn @ 1064 nm
*KH_2PO_4[6]	*Im2d*	isolated PO_4	0.034
Cs_2LiPO_4[7]	*Cmc2_1*	isolated PO_4	<0.01
$KLa(PO_3)_4$[8]	*P2_1*	$[PO_3]_\infty$ chains	0.008
$CsLa(PO_3)_4$[9]	*P2_1*	$[PO_3]_\infty$ chains	0.006
$K_4Mg_4(P_2O_7)_3$[10]	*Pc*	P_2O_7 dimer	0.007
$Rb_4Mg_4(P_2O_7)_3$[10]	*Amm2*	P_2O_7 dimer	0.009

*experimental data
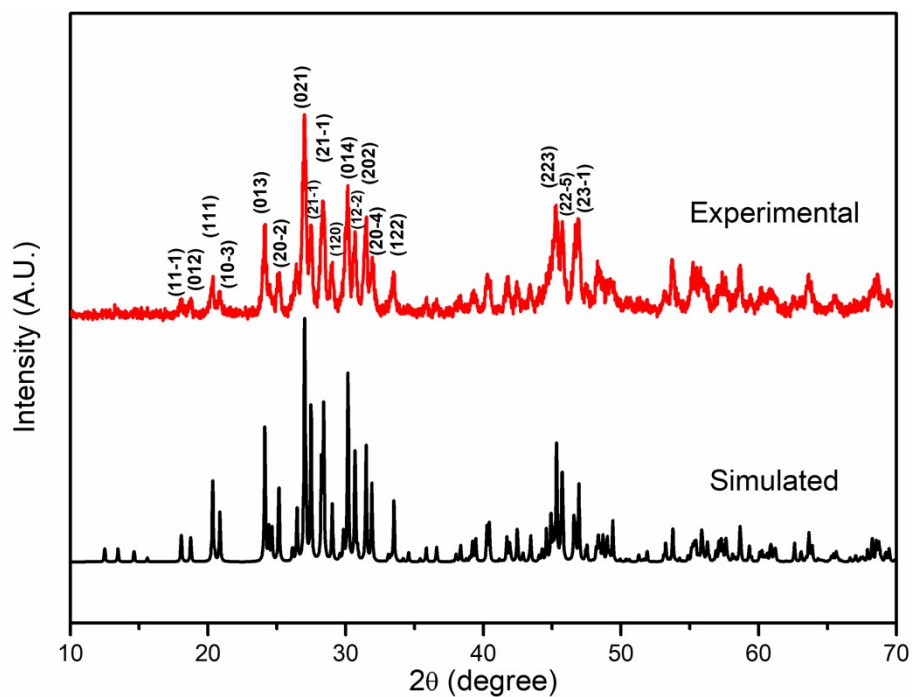
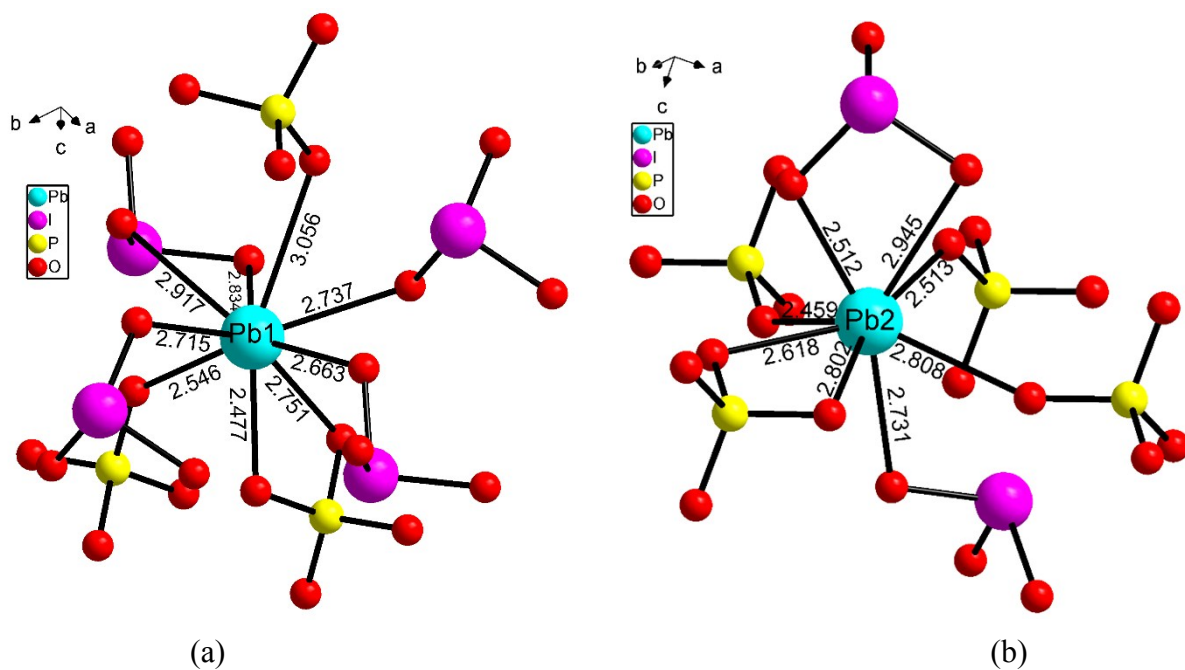**Figure S1.** The experimental and simulated powder X-ray diffraction (PXRD) patterns of $Pb_2(PO_4)(IO_3)$.

(a)   (b)

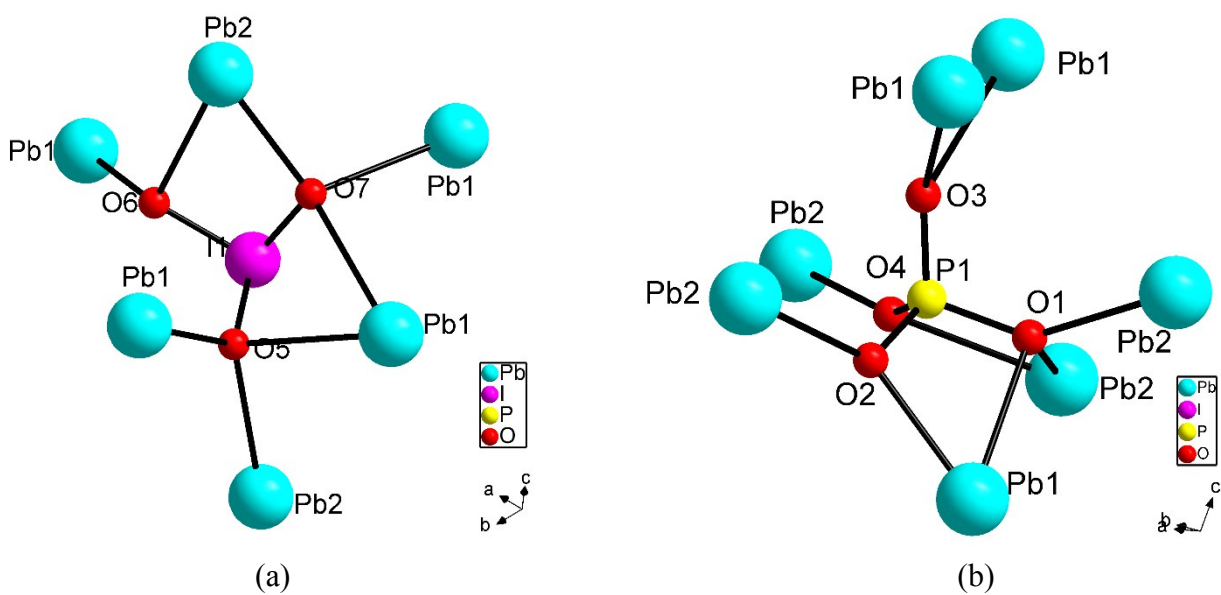**Figure S2.** The $Pb(1)O_9$ (a) and $Pb(2)O_8$ (b) coordination environments of Pb^{2+} cations.

Figure S3. The coordination modes of $(IO_3)^-$ (a) and $(PO_4)^{3-}$ (b) anions.

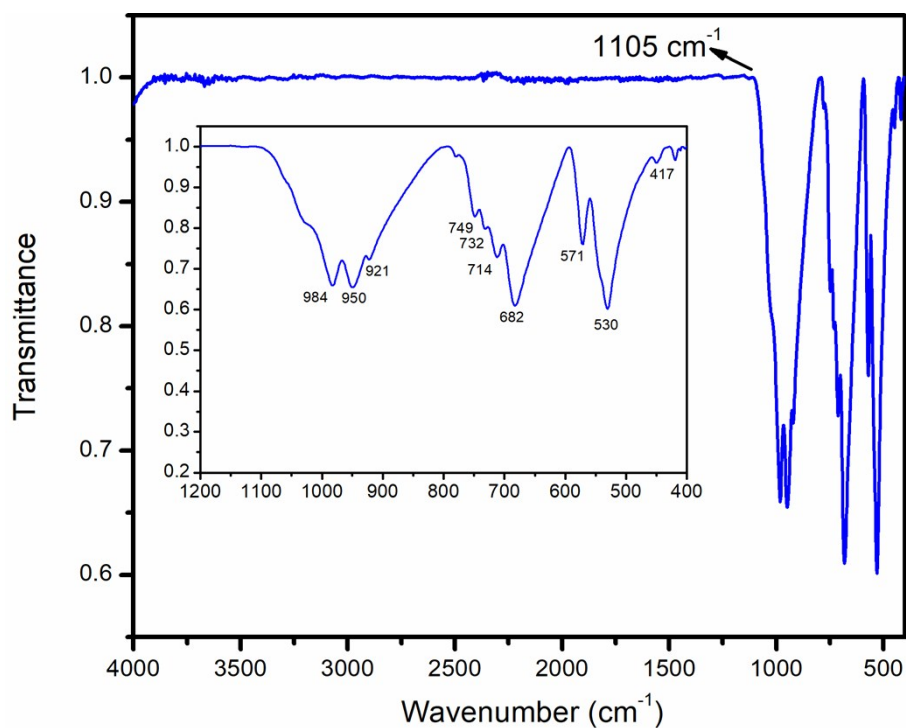**Figure S4**. Infrared spectrum of $Pb_2(PO_4)(IO_3)$.

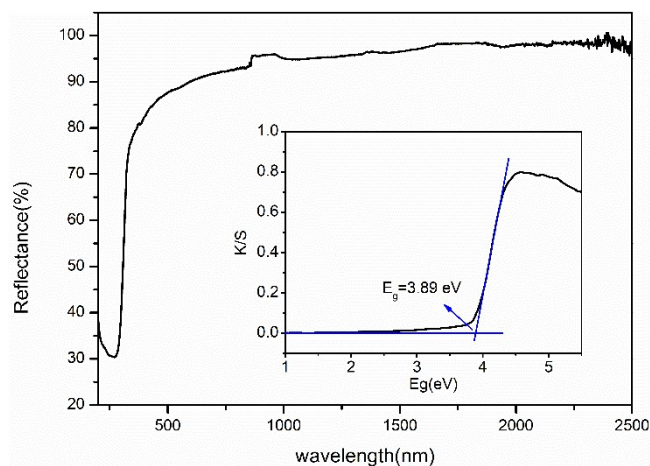**Figure S5**. UV−Vis−NIR diffuse reflectance spectrum of $Pb_2(IO_3)(PO_4)$.
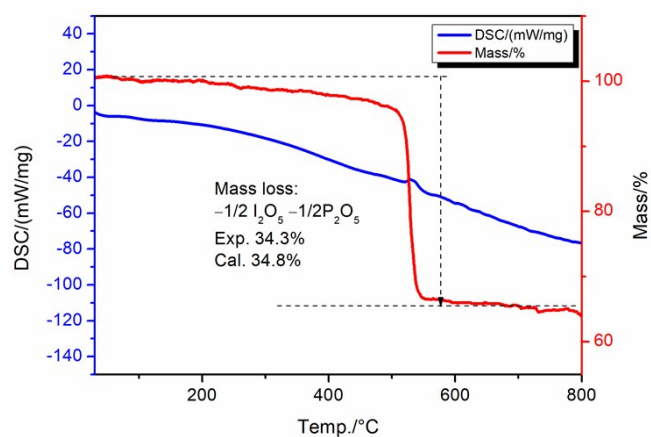
Figure S6. TGA and DSC curves of $Pb_2(IO_3)(PO_4)$.
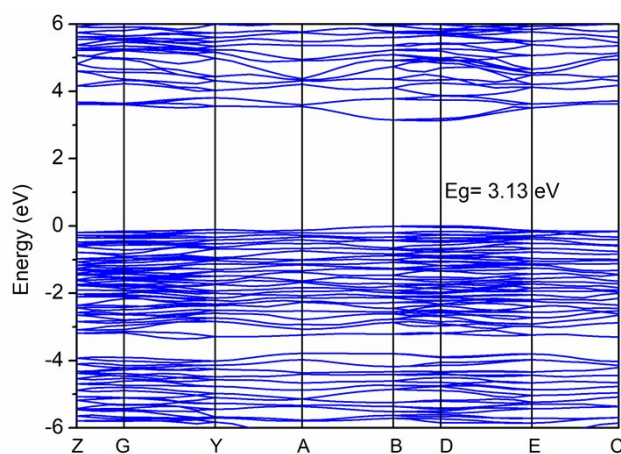
Figure S7. Calculated band structure of $Pb_2(IO_3)(PO_4)$.
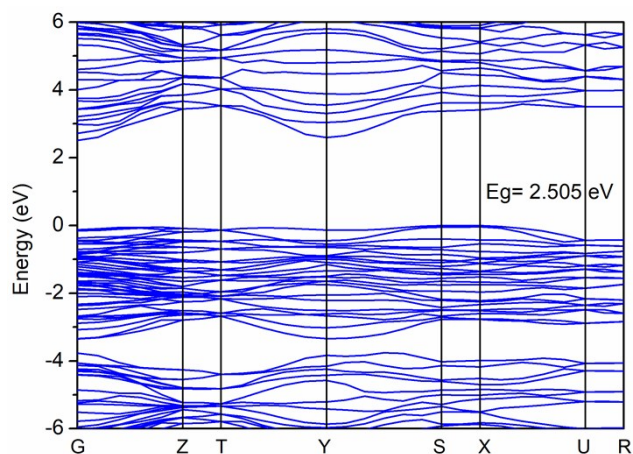
Figure S8. Calculated band structure of Pb(IO$_3$)$_2$.

Figure S9. Calculated total and partial density of states for Pb(IO$_3$)$_2$.

Figure S10. Calculated refractive indices and birefringence of Pb(IO$_3$)$_2$.

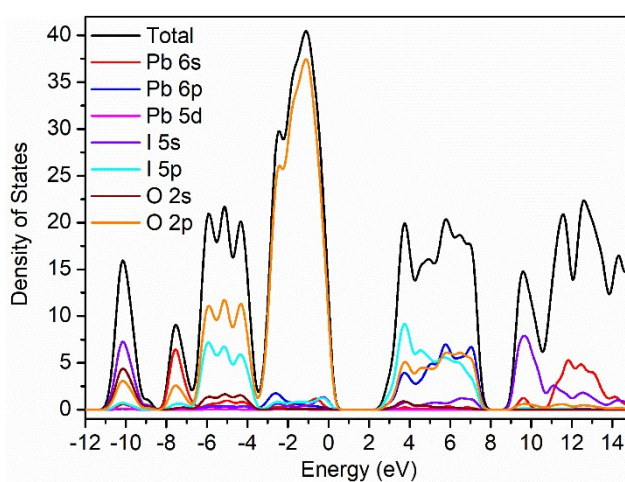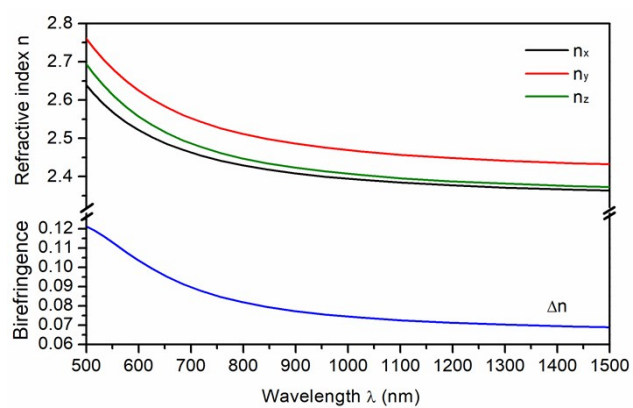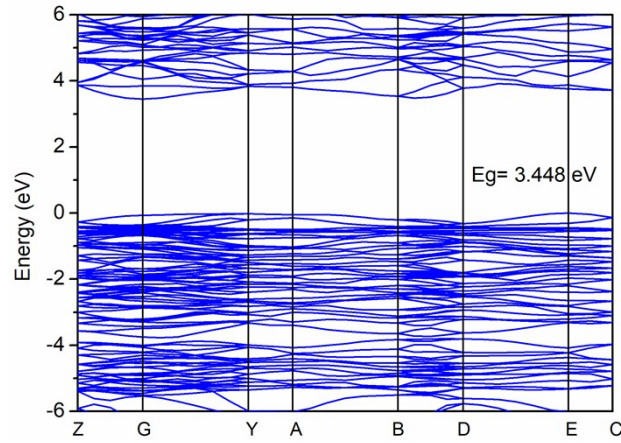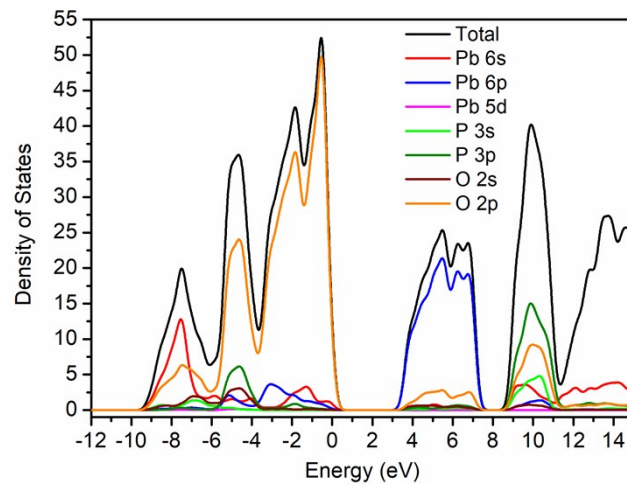**Figure S11**. Calculated band structure of $Pb_3(PO_4)_2$.

Figure S12. Calculated total and partial density of states for $Pb_3(PO_4)_2$.

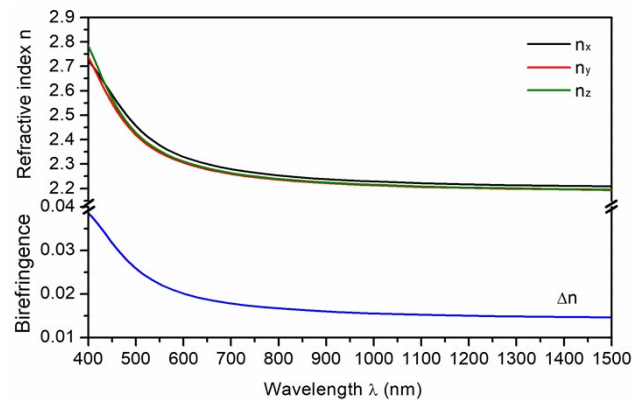**Figure S13**. Calculated refractive indices and birefringence of $Pb_3(PO_4)_2$.

Figure S14. Photograph of $Pb_2(IO_3)(PO_4)$ for the measurement of birefringence.

S15. Computational Method.

Calculations of electronic structure and optical properties for $Pb_2(PO_4)(IO_3)$ were performed using CASTEP based on density function theory (DFT).[11,12] Norm-conserving pseudopotential was used to treat the electron-core interactions, and GGA-PBE was chosen as exchange-correlation function.[13,14] The following orbital electrons were treated as valence electrons: Pb $5d^{10}6s^26p^2$, P $3s^23p^3$, I $5s^25p^5$, and O $2s^22p^4$. The Monkhorst-Pack k-point sampling of $4 \times 4 \times 2$ and a cutoff energy of 820 eV was adopted for $Pb_2(PO_4)(IO_3)$. The Monkhorst-Pack k-point sampling of $1 \times 4 \times 4$ and a cutoff energy of 820 eV was adopted for $Pb(IO_3)_2$. The Monkhorst-Pack k-point sampling of $2 \times 4 \times 3$ and a cutoff energy of 820 eV was adopted for $Pb_3(PO_4)_2$.

Based on the scissor-corrected electron band structure, the imaginary part of the dielectric function was calculated according to the electron transition from the valence bands (VB) to conduction band (CB). Consequently, the real part of the dielectric function is obtained by the Kramers-Kronig transform [15] and the calculated refractive index is determined.

References:
1.   R. C. Clark and J. S. Reid, *Acta Crystallogr., Sect. A: Found. Crystallogr.*, 1995, **51**, 887-897.
2.   O. V. Dolomanov, L. J. Bourhis, R. J. Gildea, J. A. K. Howard and H. Puschmann, *J. Appl. Crystallogr.*, 2009, **42**, 339-341.
3.   G. M. Sheldrick, *Acta Crystallogr A Found Adv*, 2015, **71**, 3-8.
4.   G. M. Sheldrick, *Acta Crystallogr C Struct Chem*, 2015, **71**, 3-8.
5.   A. L. Spek, *Acta Crystallogr C*, 2015, **71**, 9-18.
6.   D. Eimerl, *Ferroelectrics*, 1987, **72**, 397-441.
7.   B. B. Zhang, G. P. Han, Y. Wang, X. L. Chen, Z. H. Yang and S. L. Pan, *Chem. Mater.*, 2018, **30**, 5397-5403.
8.   P. Shan, T. Q. Sun, H. Chen, H. D. Liu, S. L. Chen, X. W. Liu, Y. F. Kong and J. J. Xu, *Sci Rep-Uk*, 2016, **6**.
9.   T. Q. Sun, P. Shan, H. Chen, X. W. Liu, H. D. Liu, S. L. Chen, Y. A. Cao, Y. F. Kong and J. J. Xu, *Crystengcomm*, 2014, **16**, 10497-10504.
10.   H. W. Yu, J. Young, H. P. Wu, W. G. Zhang, J. M. Rondinelli and P. S. Halasyamani, *Chem. Mater.*, 2017, **29**, 1845-1855.
11.   M. D. Segall, P. J. D. Lindan, M. J. Probert, C. J. Pickard, P. J. Hasnip, S. J. Clark and M. C. Payne, *J Phys-Condens Mat*, 2002, **14**, 2717-2744.
12.   V. Milman, B. Winkler, J. A. White, C. J. Pickard, M. C. Payne, E. V. Akhmatskaya and R. H. Nobes, *Int. J. Quantum Chem.*, 2000, **77**, 895-910.
13.   J. P. Perdew, K. Burke and M. Ernzerhof, *Phys. Rev. Lett.*, 1996, **77**, 3865-3868.
14.   J. S. Lin, A. Qteish, M. C. Payne and V. Heine, *Phys Rev B*, 1993, **47**, 4174-4180.
15.   E. D. Palik, *Journal of the Optical Society of America a-Optics Image Science and Vision*, 1984, **1**, 1297-1297.